nature materials

LETTERS

PUBLISHED ONLINE: 22 FEBRUARY 2009 | DOI: 10.1038/NMAT2398

Biodegradable luminescent porous silicon nanoparticles for *in vivo* applications

Ji-Ho Park[1,2], Luo Gu[1], Geoffrey von Maltzahn[3], Erkki Ruoslahti[4], Sangeeta N. Bhatia[3,5,6] and Michael J. Sailor[1,2,7]*

Nanomaterials that can circulate in the body hold great potential to diagnose and treat disease[1-4]. For such applications, it is important that the nanomaterials be harmlessly eliminated from the body in a reasonable period of time after they carry out their diagnostic or therapeutic function. Despite efforts to improve their targeting efficiency, significant quantities of systemically administered nanomaterials are cleared by the mononuclear phagocytic system before finding their targets, increasing the likelihood of unintended acute or chronic toxicity. However, there has been little effort to engineer the self-destruction of errant nanoparticles into non-toxic, systemically eliminated products. Here, we present luminescent porous silicon nanoparticles (LPSiNPs) that can carry a drug payload and of which the intrinsic near-infrared photoluminescence enables monitoring of both accumulation and degradation *in vivo*. Furthermore, in contrast to most optically active nanomaterials (carbon nanotubes, gold nanoparticles and quantum dots), LPSiNPs self-destruct in a mouse model into renally cleared components in a relatively short period of time with no evidence of toxicity. As a preliminary *in vivo* application, we demonstrate tumour imaging using dextran-coated LPSiNPs (D-LPSiNPs). These results demonstrate a new type of multifunctional nanostructure with a low-toxicity degradation pathway for *in vivo* applications.

The *in vivo* use of nanomaterials as therapeutic and diagnostic agents is of intense interest owing to their unique properties such as large specific capacity for drug loading[2], strong superparamagnetism[3], efficient photoluminescence[1,5] or distinctive Raman signatures[4], among others. Materials with sizes in the range of 20–200 nm can avoid renal filtration, leading to prolonged residence time in the blood stream that enables more effective targeting of diseased tissues. Many biodegradable polymeric nanoparticles that can encapsulate hydrophilic or hydrophobic drugs have been developed for *in vivo* therapeutic applications[2,6,7], and some of them have been approved for clinical use. However, organic molecule-based nanoparticles generally require the addition of a molecular tag to enable *in vivo* monitoring by fluorescence. Although carbon nanotubes, gold nanoparticles and quantum dots have demonstrated potential for *in vivo* imaging owing to their unique optical properties[1,4,8], clinical translation has been impeded owing to concerns regarding the biodegradability of such materials[4,8,9], the toxicity of degradation by-products[10] or the toxic structural characteristics of the nanomaterials themselves[11]. Although efficient renal clearance can mitigate toxic effects, optimized formulations can leave significant residual heavy metals or other toxic constituents in mononuclear phagocytic system (MPS) organs[4,12]. Furthermore, the hydrodynamic size required for renal clearance (<5.5 nm; ref. 12) may be too small to enable the incorporation of functional components such as multivalent targeting ligands, and rapid renal excretion reduces the time available to the nanomaterial to carry out its function. A more desirable design criterion for improving the biocompatibility of nanomaterials would involve the incorporation of controllable rates of self-destruction, through which components could be hierarchically degraded into harmless, renally cleared products after carrying out their *in vivo* function.

Electrochemically etched porous silicon has exhibited considerable potential for biological applications owing to its biocompatibility[13], biodegradability[14], encoding property for multiplexed detection[15] and tunable porous nanostructure for drug delivery[16]. Furthermore, since the discovery of photoluminescence of porous silicon in 1990 (ref. 17), luminescent (porous) silicon nanoparticles have been produced by several methods[18–22], some of which are amenable to biological applications[21,22]. For *in vivo* use, silicon nanoparticles provide attractive chemical alternatives to heavy-metal-containing quantum dots, which have been shown to be toxic in biological environments[10]. In addition, silicon is a common trace element in humans and a biodegradation product of porous silicon, orthosilicic acid ($Si(OH)_4$), is the form predominantly absorbed by humans and is naturally found in numerous tissues. Furthermore, silicic acid administered to humans is efficiently excreted from the body through the urine[23]. Here, we show that porous silicon nanostructures with intrinsic near-infrared luminescence can be used for *in vivo* monitoring, they can be loaded with therapeutics and they can be engineered to degrade *in vivo* into benign components that clear renally within specific timescales (Fig. 1a).

Luminescent porous Si nanoparticles (LPSiNPs) were prepared by electrochemical etching of single-crystal silicon wafers in ethanolic HF solution, lift-off of the porous silicon film, ultrasonication, filtration of the formed particles through a 0.22 μm filtration membrane and finally activation of luminescence in an aqueous solution (see Supplementary Fig. S1). During the activation step, silicon oxide grows on the hydrogen-terminated porous silicon surface, generating significant luminescence attributed to quantum confinement effects and to defects localized at the $Si–SiO_2$ interface (see Supplementary Figs S2,S3)[5,18,19]. The preparation conditions

[1]Department of Chemistry and Biochemistry, University of California, San Diego, La Jolla, California 92093, USA, [2]Materials Science and Engineering Program, University of California, San Diego, La Jolla, California 92093, USA, [3]Harvard-MIT Division of Health Sciences and Technology, Massachusetts Institute of Technology, Cambridge, Massachusetts 02139, USA, [4]Burnham Institute for Medical Research at UCSB, University of California, Santa Barbara, California 93106, USA, [5]Electrical Engineering and Computer Science, Massachusetts Institute of Technology, Cambridge, Massachusetts 02139, USA, [6]Division of Medicine, Brigham and Women's Hospital, Boston, Massachusetts 02115, USA, [7]Department of Bioengineering, University of California, San Diego, La Jolla, California 92093, USA. *e-mail: msailor@ucsd.edu.

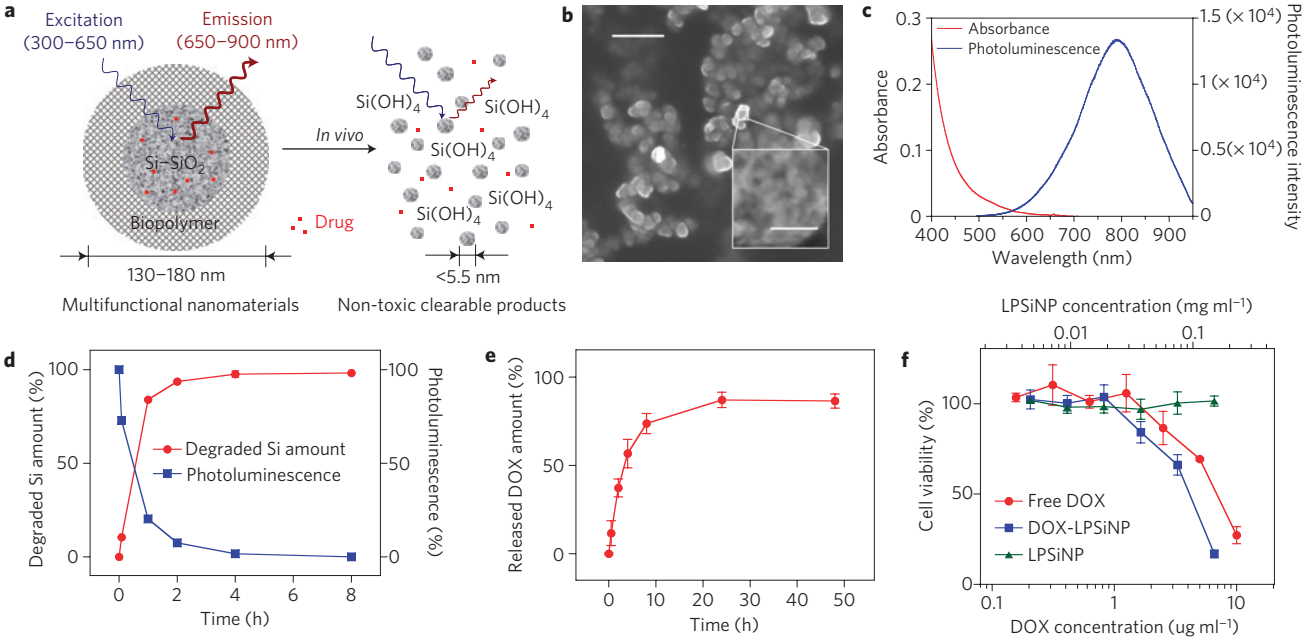

Figure 1 | Characterization of LPSiNPs. a, Schematic diagram depicting the structure and *in vivo* degradation process for the (biopolymer-coated) nanoparticles used in this study. **b**, SEM image of LPSiNPs (the inset shows the porous nanostructure of one of the nanoparticles). The scale bar is 500 nm (50 nm for the inset). **c**, Photoluminescence emission and absorbance spectra of LPSiNPs. Photoluminescence is measured using ultraviolet excitation ($\lambda = 370$ nm). **d**, Appearance of silicon in solution (by ICP-OES) and photoluminescence intensity ($\lambda_{ex} = 370$ nm and λ_{em} = maximum peak intensity at each time point) from a sample of LPSiNPs (50 μg ml^{-1}) incubated in PBS solution at 37 °C as a function of time. **e**, Release profile depicting per cent of DOX from DOX-LPSiNPs released into a PBS solution as a function of time at 37 °C. Data were obtained by filtering out DOX-LPSiNPs from the solution at each time point using a centrifugal filter and measuring the fluorescence intensity of free DOX left in solution ($\lambda_{em} = 590$ nm, $\lambda_{ex} = 480$ nm). **f**, Cytotoxicity of DOX-LPSiNPs, bare LPSiNPs and free DOX towards MDA-MB-435 human carcinoma cells, quantified by the MTT assay. The cells were incubated with the samples for 48 h. The error bars in **d** and **f** indicate s.d.

were optimized to provide pore volume and surface area suitable for loading of therapeutics and long *in vivo* circulation times while maintaining an acceptable degradation rate (see Supplementary Figs S4,S5). As a result, the medium-sized (126 nm) particles prepared by electrochemical etching at 200 mA cm^{-2} for 150 s were chosen for the study presented here. The LPSiNPs appear spherical and fairly uniform in the scanning electron microscope (SEM), with a well-defined micro- and meso-porous nanostructure (Fig. 1b). The pore diameters are of the order of 5–10 nm (see Supplementary Fig. S4a,b). The mean hydrodynamic size measured by dynamic light scattering is ~126 nm, consistent with the SEM measurements.

The intrinsic photoluminescence of LPSiNPs under ultraviolet excitation appears at wavelengths between 650 and 900 nm (Fig. 1c), suitable for *in vivo* imaging owing to low tissue adsorption in this spectral range[24]. The materials exhibit greater photostability relative to fluorescein or the well-known near-infrared cyanine fluorophores, Cy5.5 and Cy7 (see Supplementary Fig. S6). The quantum yield of LPSiNPs in ethanol was determined to be ~10.2% (relative to Rhodamine 101 standard) (see Supplementary Fig. S7), which is in accord with previously reported values for other water-soluble luminescent silicon–silica nanoparticles[21,22]. When placed in biological solution (phosphate buffered saline (PBS), pH 7.4, 37 °C) at a mass concentration less than the solubility of silicic acid (0.1 ~ 0.2 mg ml^{-1} SiO_2; ref. 25), LPSiNPs lose their luminescence in a short time and dissolve (Fig. 1d). A blueshift of the luminescence spectrum during degradation is indicative of a shrinking in size of the semiconductor fluorophore (see Supplementary Fig. S8). No detectable (by dynamic light scattering) LPSiNPs remain after 8 h of incubation. However, degradation is slowed by addition of a molecular or polymeric surface coating (see below).

The anti-cancer drug doxorubicin (DOX) was incorporated into the LPSiNPs (DOX-LPSiNPs, ~43.8 μg DOX per 1 mg LPSiNP) to test their potential for therapeutic applications (see Supplementary Fig. S9). The positively charged DOX molecules are bound to the negatively charged porous SiO_2 surface by electrostatic forces. Loading of DOX increases the zeta potential of the nanoparticles from −52 to −39 mV. A relatively slow release of the drug is observed at physiological pH and temperature, reaching significant levels within 8 h (Fig. 1e). The appearance of free silicic acid in solution as a function of time, indicative of degradation of the LPSiNPs, correlates with the DOX release profile. The rate of degradation of DOX-LPSiNPs is somewhat slower than bare LPSiNPs (see Supplementary Fig. S9a). We postulate that the presence of DOX molecules inhibits the nanoparticle dissolution process by slowing the rate of SiO_2 hydrolysis at the LPSiNP surface.

DOX-LPSiNPs exhibit similar or slightly greater cytotoxicity relative to free DOX, whereas bare LPSiNPs show no significant cytotoxicity (Fig. 1f). It is possible that silicic acid released by the LPSiNPs increases the cytotoxicity of DOX by decreasing local extracellular or intracellular pH (ref. 26). In a preliminary *in vivo* study (see Supplementary Fig. S9b–d), DOX-LPSiNPs exhibited similar circulation times to bare LPSiNPs, suggesting that the adsorbed DOX molecules have no significant effect on LPSiNP circulation, in contrast to the rapid clearance observed with nanoparticles that are coated with positively charged polymer/peptide[27]. Importantly, DOX-LPSiNPs retained DOX molecules during circulation and delivered them to organs related to nanoparticle clearance such as the liver and the spleen. Previous work has shown that sequestration of DOX (in that case, in liposomes) reduces cardiotoxicity by reducing the systemic concentration of free DOX (ref. 26).

Next, we tested biodegradability and biocompatibility of LPSiNPs *in vitro* and *in vivo*. The LPSiNP formulation is relatively non-toxic to HeLa cells *in vitro* within the tested concentration range (Fig. 2a and Supplementary Figs S4e,S5c,S10). For *in vivo*

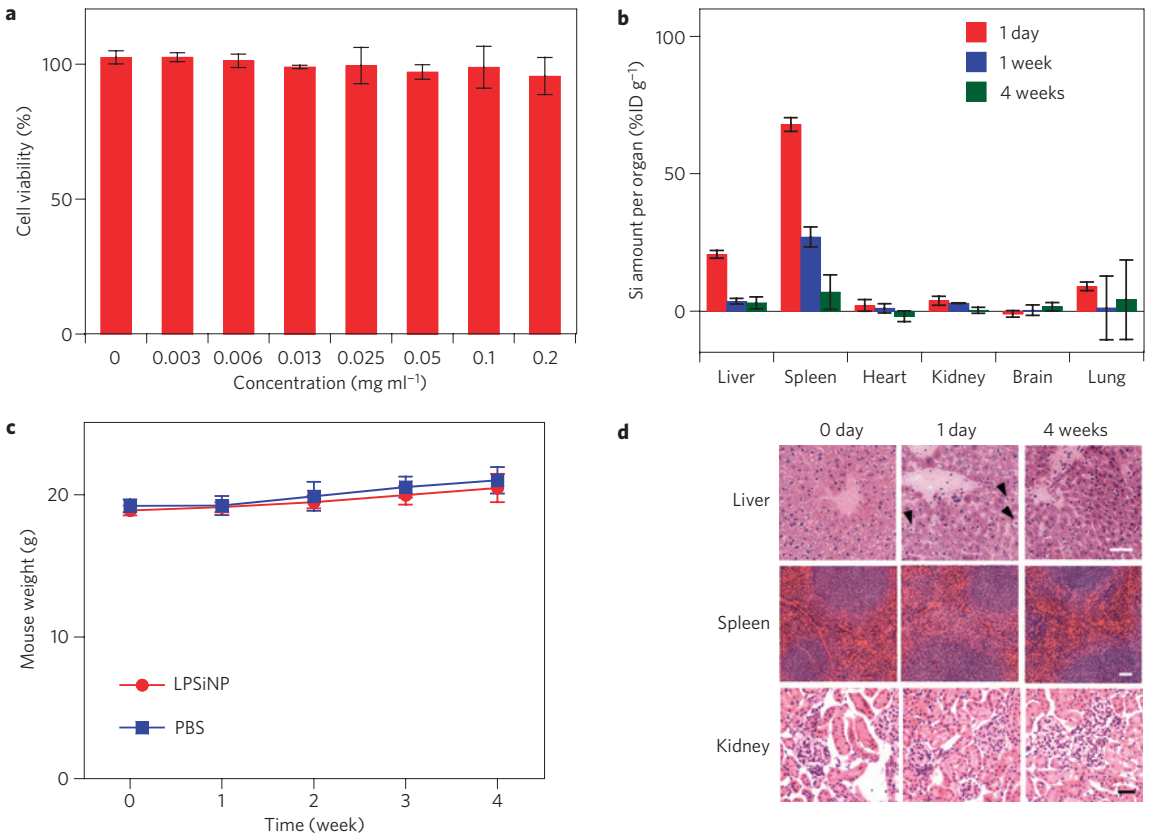

Figure 2 | Biocompatibility and biodegradability of LPSiNPs. a, *In vitro* cytotoxicity of LPSiNP towards HeLa cells, determined by the calcein assay. LPSiNPs at the indicated concentrations were incubated with cells for 48 h. **b**, *In vivo* biodistribution and biodegradation of LPSiNPs over a period of 4 weeks in a mouse. Aliquots of LPSiNPs were intravenously injected into the mouse ($n = 3$ or 4, dose = 20 mg kg^{-1}). The silicon concentration in the organs was determined at different time points after injection using ICP-OES. **c**, Change in body mass of mice injected with LPSiNPs ($n = 3$, dose = 20 mg kg^{-1}) compared with PBS control ($n = 4$). There is no statistically significant difference in the mass change between control (PBS) and LPSiNPs over a period of 4 weeks. The error bars in **a**–**c** indicate s.d. **d**, Liver, spleen and kidney histology. Livers, spleens and kidneys were collected from mice before, 1 day and 4 weeks after intravenous injection of LPSiNPs (20 mg kg^{-1}). Organs were stained with haematoxylin and eosin. The arrows indicate the LPSiNPs taken up by macrophages in the liver. The scale bar is 50 μm for all images.

studies, LPSiNPs (20 mg kg^{-1}) were injected intravenously into mice. As with many other nanomaterials[3,4,12], the injected LPSiNPs accumulate mainly in the MPS-related organs such as the liver and the spleen (Fig. 2b). However, the LPSiNPs accumulated in the organs are noticeably cleared from the body within a period of 1 week and completely cleared in 4 weeks. The mechanism of clearance is attributed to degradation into soluble silicic acid followed by excretion. This result contrasts with the slow clearance generally observed for other types of inorganic nanoparticle with diameters >5.5 nm (refs 4,8,9). Over a period of 4 weeks, the body weight of the mice injected with LPSiNPs increased slightly in a pattern similar to the control mice (Fig. 2c), indicating that the mice continue to mature without any significant toxic effects.

As the degradation of highly localized LPSiNPs may induce subsequent damage in the organs related to nanoparticle clearance, *in vivo* toxicity of LPSiNPs was further examined in kidney, liver and spleen tissues of mice 1 day and 4 weeks after LPSiNP injection. Histopathologically, no significant toxicity was observed in these tissues relative to the controls (Fig. 2d). Hepatocytes in the liver samples appeared unremarkable, and there were no inflammatory infiltrates. However, the sinusoids in between the rows of hepatocytes contained Kupffer cells (macrophages) that appeared swollen 1 day after injection. The cells returned to the normal morphology 4 weeks after injection, implying that LPSiNPs were taken up, degraded (presumably by lysosomes) and the soluble products were subsequently released from the cells. Spleen samples showed no significant change in morphology of the lymphoid follicles or in the size of the red pulp after LPSiNP injection. Kidney samples also showed no remarkable change in the morphology. Although the *in vivo* toxicity results shown here are preliminary, the LPSiNPs show promise as non-toxic biodegradable inorganic nanomaterials.

We next investigated the possibility of imaging cells *in vitro* and organs *in vivo* using the intrinsic photoluminescent properties of LPSiNPs. Significant luminescence of LPSiNPs was observed in HeLa cells using excitation wavelengths of 370, 488 and 750 nm (two-photon excitation) 2 h after incubation, attributed to non-specific cellular uptake of the silica-based nanomaterials[28] (Fig. 3a and Supplementary Fig. S11). To examine their potential for *in vivo* imaging, subcutaneous and intramuscular injections of LPSiNP dispersions (20 μl aliquots, 0.1 mg ml^{-1}) into the left and right flank of a nude mouse, respectively, were administered. The mouse was imaged in a fluorescence mode (green fluorescent protein (GFP) excitation filter, 445–490 nm and indocyanine green (ICG) emission filter, 810–875 nm). The signals from both injections were clearly observed without any skin autofluorescence, although the near-skin fluorescence intensity is larger than the signal emanating from deeper tissue (Fig. 3b). The fluorescence spectrum of LPSiNPs enables imaging in the near-infrared-emission range, a convenient window for *in vivo* imaging owing to the low levels of near-infrared autofluorescence of mouse skin excited with visible light[1,29].

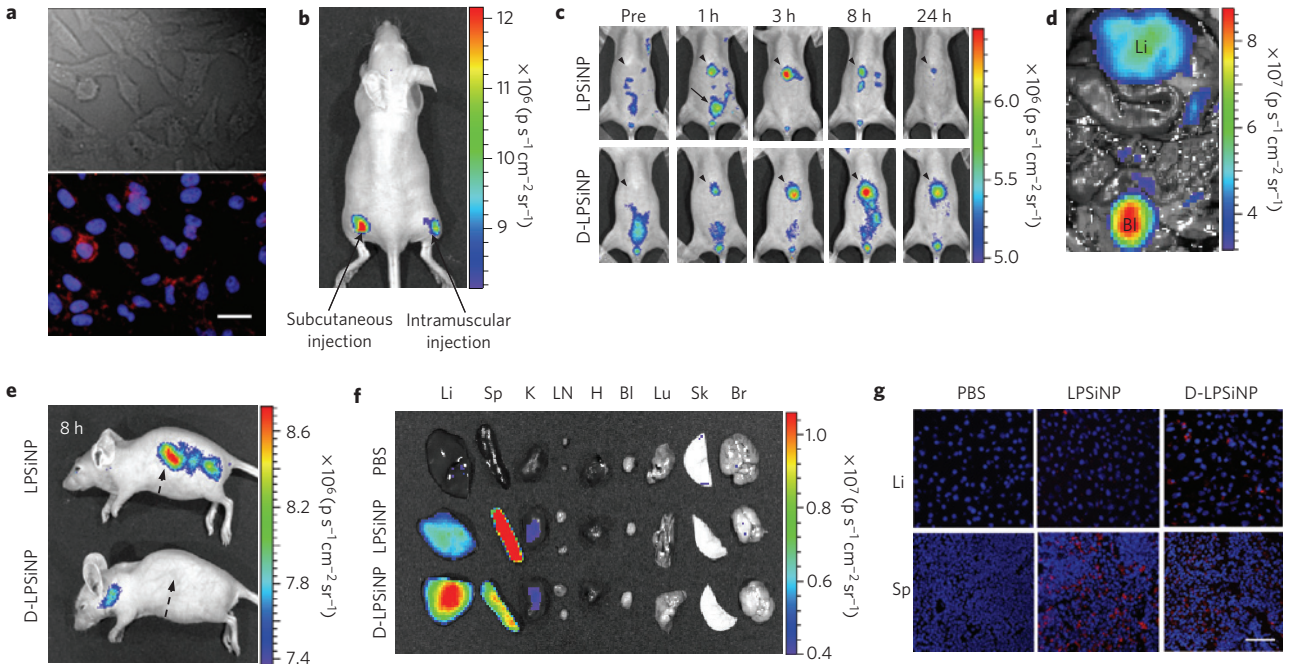

Figure 3 | *In vitro, in vivo* and *ex vivo* fluorescence imaging with LPSiNPs. a, *In vitro* cellular imaging with LPSiNPs. HeLa cells were treated with LPSiNPs for 2 h and then imaged. Red and blue indicate LPSiNPs and cell nuclei, respectively. The scale bar is 20 μm. **b**, *In vivo* fluorescence image of LPSiNPs (20 μl of 0.1 mg ml^{-1}) injected subcutaneously and intramuscularly on each flank of a mouse. **c**, *In vivo* images of LPSiNPs and D-LPSiNPs. The mice were imaged at multiple time points after intravenous injection of LPSiNPs and D-LPSiNPs (20 mg kg^{-1}). Arrowheads and arrows with solid lines indicate liver and bladder, respectively. **d**, *In vivo* image showing the clearance of a portion of the injected dose of LPSiNPs into the bladder, 1 h post-injection. Li and Bl indicate liver and bladder, respectively. **e**, Lateral image of the same mice shown in **c**, 8 h after LPSiNP or D-LPSiNP injection. Arrows with dashed lines indicate spleen. **f**, Fluorescence images showing the *ex vivo* biodistribution of LPSiNPs and D-LPSiNPs in a mouse. Organs were collected from the animals shown in **c**, 24 h after injection. Li, Sp, K, LN, H, Bl, Lu, Sk and Br indicate liver, spleen, kidney, lymph nodes, heart, bladder, lung, skin and brain, respectively. **g**, Fluorescence histology images of livers and spleens from the mice shown in **c** and **f**, 24 h after injection. Red and blue indicate (D-)LPSiNPs and cell nuclei, respectively. The scale bar is 50 μm for all images.

We next examined whole-body fluorescence imaging of nude mice using LPSiNPs administered by intravenous injection. To prevent rapid degradation after injection and to increase their blood half-life, LPSiNPs were coated with the biopolymer dextran by physisorption[30] (D-LPSiNP, Supplementary Fig. S12). The coating process increased the size and zeta potential of the nanoparticles (from 125 nm to 151 nm and from −52 mV to −43.5 mV, respectively). Bare LPSiNPs or D-LPSiNPs were injected and imaged at different time points (Fig. 3c–e). A significant fraction of the bare LPSiNPs were immediately removed by renal clearance, presumably owing to their degradation into smaller (<5.5 nm) nanoparticles[12]. The remaining nanoparticles were observed to accumulate in the liver and the spleen, consistent with the histology data discussed above.

The D-LPSiNPs exhibit a somewhat different pattern in their uptake by the MPS-related organs. These nanoparticles accumulate and degrade in the liver slowly relative to bare LPSiNPs, which is consistent with the *in vitro* degradation and *in vivo* blood half-life data (see Supplementary Fig. S12c,d). Biodistribution and histological studies of the organs collected from the same mice 24 h after injection are consistent with the whole-body fluorescence imaging data (liver < spleen for LPSiNPs and liver > spleen for D-LPSiNPs) (Fig. 3f,g). These results indicate that the intrinsic luminescent properties of LPSiNPs enable the non-invasive monitoring of their biodistribution and degradation in a live animal as well as the microscopic observation of their localization in the organs.

Last, we evaluated the potential of LPSiNPs to image tumours *in vivo*. To detect and image deep-tissue diseases such as tumours by fluorescence, the excitation wavelength for the nanoparticle should be in the near-infrared range to maximize tissue penetration and minimize optical absorption by physiologically abundant species such as haemoglobin[24]. LPSiNPs emit in the near-infrared (810–875 nm) and they can be excited with red or near-infrared radiation (615–665 nm or 710–760 nm) (Fig. 4a) or by two-photon near-infrared excitation (see Supplementary Fig. S11). Similar to some of the near-infrared-emitting semiconductor quantum dots[29], the quantum efficiency of LPSiNPs decreases with longer excitation wavelengths. However, the quantum yield is sufficient to enable their observation in internal organs using a conventional fluorescence imaging system.

Injection of the D-LPSiNP formulation (20 mg kg^{-1}) into a nude mouse bearing an MDA-MB-435 tumour results in passive accumulation of the nanomaterial in the tumour, as revealed in the near-infrared fluorescence image (Fig. 4b). Imaging with shorter excitation wavelengths (blue or green filter sets) results in poor differentiation of the target organ relative to the surrounding skin area (see Supplementary Fig. S13). The *ex vivo* fluorescence images and histology confirm the presence of D-LPSiNPs in the tumour (Fig. 4c,d).

This study represents the first example of the imaging of a tumour and other organs using biodegradable silicon nanoparticles in live animals, and it is important because of the biodegradability and low *in vivo* toxicity observed. The LPSiNPs injected intravenously are observed to accumulate mainly in MPS-related organs and are degraded *in vivo* into apparently non-toxic products within a few days and removed from the body through renal clearance. These larger (100 nm-scale) silicon-based biodegradable nanoparticles overcome many of the disadvantages of smaller (<5.5 nm) nanocrystals[12] such as fast clearance from circulation, low capacity

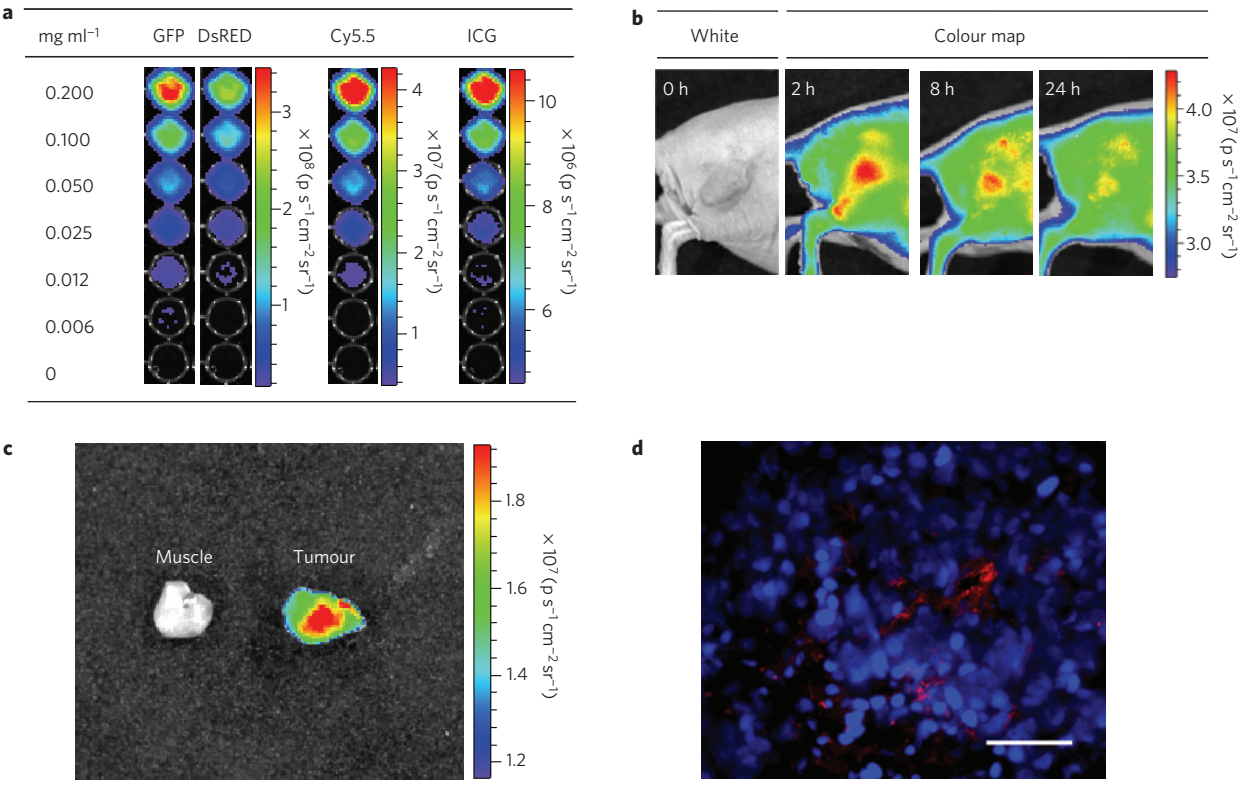

Figure 4 | Fluorescence images of tumours containing D-LPSiNPs. a, Fluorescence images of D-LPSiNPs as a function of concentration using different excitation filters (GFP: 445–490 nm and 1 s exposure time; Discosoma red fluorescent protein (DsRed): 500–550 nm, 2 s exposure time; Cy5.5: 615–665 nm, 8 s exposure time; ICG: 710–760 nm, 20 s exposure time). The emission filter used is ICG (810–875 nm). **b**, Representative fluorescence images of a mouse bearing an MDA-MB-435 tumour. The mouse was imaged using a Cy5.5 excitation filter and an ICG emission filter at the indicated times after intravenous injection of D-LPSiNPs (20 mg kg^{-1}). Note that a strong signal from D-LPSiNPs is observed in the tumour, indicating significant passive accumulation in the tumour by the enhanced permeability and retention (EPR) effect. **c**, *Ex vivo* fluorescence images of tumour and muscle around the tumour from the mouse used in **b**. **d**, Fluorescence images of a tumour slice from the mouse in **b**. Red and blue indicate D-LPSiNPs and cell nuclei (DAPI stain), respectively. The scale bar is 100 μm.

for drug loading and toxicity of the residual particles that do not escape MPS uptake[4,12]. We believe the reduced *in vivo* toxicity of this multifunctional inorganic nanomaterial provides a promising pathway for clinical translation.

Methods

Preparation of LPSiNPs. Porous silicon samples were prepared by electrochemical etching of a p^{++}-type silicon wafer by application of a constant current density of 200 mA cm^{-2} for 150 s in an aqueous HF/ethanol electrolyte. A freestanding film of the porous silicon nanostructure was then removed from the crystalline silicon substrate by application of a current pulse of 4 mA cm^{-2} for 250 s in an aqueous HF/ethanol electrolyte. The freestanding hydrogen-terminated porous silicon film was fractured by sonication overnight, and then filtered through a 0.22 μm filtration membrane (Millipore). The nanoparticles were further incubated in deionized water for ~2 weeks to activate their luminescence in the near-infrared range. For dextran-coated LPSiNPs (D-LPSiNPs), dextran (MW ~ 20000, Sigma) was physically absorbed on LPSiNPs.

Nanoparticle characterization. SEM micrographs were obtained with a Hitachi S-4800 field-emission instrument. Dynamic light scattering (Zetasizer Nano ZS90, Malvern Instruments) was used to determine hydrodynamic size and zeta potential of (D-)LPSiNPs. The photoluminescence (λ_{ex} = 370 and 460 nm long-pass emission filter) and absorbance spectra of (D-)LPSiNP were obtained using a Princeton Instruments/Acton spectrometer fitted with a liquid-nitrogen-cooled silicon charge-coupled device detector, and a Hewlett-Packard 8452A ultraviolet–visible diode array spectrophotometer, respectively. Fluorescence images of D-LPSiNPs subjected to different excitation wavelength bands were obtained using an IVIS 200 imaging system (Xenogen).

***In vitro* degradation.** (D-)LPSiNPs were incubated at 37 °C in PBS. An aliquot was removed at different time points and filtered with a centrifugal filter (30,000 Da molecular weight cutoff, Millipore) to remove undissolved LPSiNPs. The filtered solution was subjected to analysis by inductively coupled plasma optical emission spectroscopy (ICP-OES, Perkin Elmer Optima 3000DV). The decrease in photoluminescence of the above samples over time was also monitored.

Drug loading and cytotoxicity. LPSiNP was loaded with DOX (Sigma) in deionized water and then rinsed using a centrifugal filter. Release kinetics of DOX from DOX-loaded LPSiNPs (DOX-LPSiNPs) in PBS at 37 °C was measured by filtering out DOX-LPSiNPs from the solution at each time point using the centrifugal filter and measuring fluorescence of free DOX left in the solution at 590 nm (λ_{ex} = 480 nm). For drug-mediated cytotoxicity experiments, MDA-MB-435 human carcinoma cells were incubated with LPSiNPs, DOX-LPSiNPs or free DOX for 48 h. The cytotoxicity of LPSiNPs, DOX-LPSiNPs or free DOX was evaluated using the MTT (3-(4,5-dimethyl-2-thiazolyl)-2,5-diphenyltetrazolium bromide) assay (Chemicon).

***In vivo* degradation, toxicity and circulation.** All animal work was carried out in accordance with the institutional animal protocol guidelines in place at the Burnham Institute for Medical Research, and it was reviewed and approved by the Institute's Animal Research Committee. (D-)LPSiNPs were intravenously injected into BALB/c mice (20 mg kg^{-1}). For *in vivo* degradation studies, the mice were killed 1 day, 1 week and 4 weeks after injection, and the brain, heart, kidney, liver, lung and spleen were collected. The tissues were weighed, digested and then analysed for silicon content using ICP-OES. For the *in vivo* toxicity studies, the mass of each mouse was monitored for 4 weeks after injection and compared with control mice (PBS-injected). The sections of kidney, liver and spleen tissues collected from the mice 1 day and 4 weeks after injection were stained with haematoxylin and eosin and then examined by a pathologist.

***In vivo* fluorescence imaging.** LPSiNPs were injected subcutaneously and intramuscularly into the left and right flank, respectively, of a nude mouse, and imaged immediately with GFP excitation (445–490 nm) and an ICG (810–875 nm) emission filter using the IVIS 200 imaging system. For systemic administration, (D-)LPSiNPs were intravenously injected into nude mice (20 mg kg^{-1}). The

mice were imaged under anaesthesia several different times after injection using the IVIS 200 imaging system. The organs (bladder, brain, heart, kidney, lymph nodes, liver, lung, skin and spleen), collected 24 h after injection, were also imaged. The excitation filter used was GFP (445–490 nm) and the emission filter used was ICG (810–875 nm). For *in vivo* fluorescence tumour imaging, a nude mouse bearing an MDA-MB-435 human carcinoma tumour (~0.5 cm, one side of flank) was used. The tumour area was imaged under anaesthesia several different times after intravenous injection of D-LPSiNPs (20 mg kg^{-1}) using the IVIS 200 imaging system. The tumour and muscle around the tumour, collected 24 h after injection, were also imaged. The excitation filter used was Cy5.5 (615–665 nm) and the emission filter used was ICG (810–875 nm). For fluorescent histological analysis, sections of liver, spleen and tumour tissues were fixed with 4% paraformaldehyde, stained with 4,6-diamidino-2-phenylindole (DAPI) and then observed with 370 nm excitation and 650 nm long-pass emission filter using the fluorescence microscope.

A full description of the methods is available in Supplementary Methods.

Received 8 September 2008; accepted 19 January 2009; published online 22 February 2009

References

1. Gao, X. H., Cui, Y. Y., Levenson, R. M., Chung, L. W. K. & Nie, S. M. *In vivo* cancer targeting and imaging with semiconductor quantum dots. *Nature Biotech.* **22**, 969–976 (2004).
2. Torchilin, V. P. Recent advances with liposomes as pharmaceutical carriers. *Nature Rev. Drug Disc.* **4**, 145–160 (2005).
3. Lee, J. H. *et al.* Artificially engineered magnetic nanoparticles for ultra-sensitive molecular imaging. *Nature Med.* **13**, 95–99 (2007).
4. Liu, Z. *et al.* Circulation and long-term fate of functionalized, biocompatible single-walled carbon nanotubes in mice probed by Raman spectroscopy. *Proc. Natl Acad. Sci. USA* **105**, 1410–1415 (2008).
5. Godefroo, S. *et al.* Classification and control of the origin of photoluminescence from Si nanocrystals. *Nature Nanotech.* **3**, 174–178 (2008).
6. Sengupta, S. *et al.* Temporal targeting of tumour cells and neovasculature with a nanoscale delivery system. *Nature* **436**, 568–572 (2005).
7. Farokhzad, O. C. *et al.* Targeted nanoparticle-aptamer bioconjugates for cancer chemotherapy *in vivo*. *Proc. Natl Acad. Sci. USA* **103**, 6315–6320 (2006).
8. Kim, D., Park, S., Lee, J. H., Jeong, Y. Y. & Jon, S. Antibiofouling polymer-coated gold nanoparticles as a contrast agent for in vivo X-ray computed tomography imaging. *J. Am. Chem. Soc.* **129**, 7661–7665 (2007).
9. Ballou, B., Lagerholm, B. C., Ernst, L. A., Bruchez, M. P. & Waggoner, A. S. Noninvasive imaging of quantum dots in mice. *Bioconjugate Chem.* **15**, 79–86 (2004).
10. Derfus, A. M., Chan, W. C. W. & Bhatia, S. N. Probing the cytotoxicity of semiconductor quantum dots. *Nano Lett.* **4**, 11–18 (2004).
11. Poland, C. A. *et al.* Carbon nanotubes introduced into the abdominal cavity of mice show asbestos-like pathogenicity in a pilot study. *Nature Nanotech.* **3**, 423–428 (2008).
12. Choi, H. S. *et al.* Renal clearance of quantum dots. *Nature Biotech.* **25**, 1165–1170 (2007).
13. Bayliss, S. C., Heald, R., Fletcher, D. I. & Buckberry, L. D. The culture of mammalian cells on nanostructured silicon. *Adv. Mater.* **11**, 318–321 (1999).
14. Canham, L. T. Bioactive silicon structure fabrication through nanoetching techniques. *Adv. Mater.* **7**, 1033–1037 (1995).
15. Cunin, F. *et al.* Biomolecular screening with encoded porous-silicon photonic crystals. *Nature Mater.* **1**, 39–41 (2002).
16. Salonen, J., Kaukonen, A. M., Hirvonen, J. & Lehto, V.-P. Mesoporous silicon in drug delivery applications. *J. Pharm. Sci.* **97**, 632–653 (2008).
17. Canham, L. T. Silicon quantum wire array fabrication by electrochemical and chemical dissolution of wafers. *Appl. Phys. Lett.* **57**, 1046–1048 (1990).
18. Heinrich, J. L., Curtis, C. L., Credo, G. M., Kavanagh, K. L. & Sailor, M. J. Luminescent colloidal silicon suspensions from porous silicon. *Science* **255**, 66–68 (1992).
19. Wilson, W. L., Szajowski, P. F. & Brus, L. E. Quantum confinement in size-selected surface-oxidized silicon nanocrystals. *Science* **262**, 1242–1244 (1993).
20. Mangolini, L. & Kortshagen, U. Plasma-assisted synthesis of silicon nanocrystal inks. *Adv. Mater.* **19**, 2513–2519 (2007).
21. Wang, L., Reipa, V. & Blasic, J. Silicon nanoparticles as a luminescent label to DNA. *Bioconjugate Chem.* **15**, 409–412 (2004).
22. Li, Z. F. & Ruckenstein, E. Water-soluble poly(acrylic acid) grafted luminescent silicon nanoparticles and their use as fluorescent biological staining labels. *Nano Lett.* **4**, 1463–1467 (2004).
23. Popplewell, J. F. *et al.* Kinetics of uptake and elimination of silicic acid by a human subject: A novel application of ^{32}Si and accelerator mass spectrometry. *J. Inorg. Biochem.* **69**, 177–180 (1998).
24. Weissleder, R. A clearer vision for in vivo imaging. *Nature Biotech.* **19**, 316–317 (2001).
25. Piryutko, M. M. The solubility of silicic acid in salt solutions. *Russ. Chem. Bull.* **8**, 355–360 (1959).
26. Minotti, G., Menna, P., Salvatorelli, E., Cairo, G. & Gianni, L. Anthracyclines: Molecular advances and pharmacologic developments in antitumor activity and cardiotoxicity. *Pharmacol. Rev.* **56**, 185–229 (2004).
27. Wunderbaldinger, P., Josephson, L. & Weissleder, R. Tat peptide directs enhanced clearance and hepatic permeability of magnetic nanoparticles. *Bioconjugate Chem.* **13**, 264–268 (2002).
28. Slowing, I., Trewyn, B. G. & Lin, V. S.-Y. Effect of surface functionalization of MCM-41-type mesoporous silica nanoparticles on the endocytosis by human cancer cells. *J. Am. Chem. Soc.* **128**, 14792–14793 (2006).
29. Kim, S. *et al.* Near-infrared fluorescent type II quantum dots for sentinel lymph node mapping. *Nature Biotech.* **22**, 93–97 (2003).
30. Suh, K. Y. *et al.* Characterization of chemisorbed hyaluronic acid directly immobilized on solid substrates. *J. Biomed. Mater. Res. B* **15**, 292–298 (2006).

Acknowledgements

This work was supported by the National Cancer Institute of the National Institutes of Health through grant numbers U54 CA 119335 (UCSD CCNE), 5-R01-CA124427 (BRP) and U54 CA119349 (MIT CCNE). M.J.S., S.N.B. and E.R. are members of the Moores UCSD Cancer Center and the UCSD NanoTUMOR Center under which this work was conducted and supported by the NIH/NCI grant. J.-H.P. thanks the Korea Science and Engineering Foundation (KOSEF) for a Graduate Study Abroad Scholarship. The authors thank Melanie L. Oakes in the Hitachi Chemical Research for assistance with SEM analysis, Edward Monosov in the Burnham Institute for Medical Research for assistance with confocal and multi-photon microscopy and Nissi Varki of the Moores UCSD Cancer Center for toxicity examination of the histology samples.

Author contributions

J.-H.P., L.G. and M.J.S. conceived and designed the research. J.-H.P. and L.G. carried out the experiments. J.-H.P., L.G., G.v.M., E.R., S.N.B. and M.J.S. analysed the data. J.-H.P. and M.J.S. wrote the manuscript.

Additional information

Supplementary Information accompanies this paper on www.nature.com/naturematerials. Reprints and permissions information is available online at http://npg.nature.com/reprintsandpermissions. Correspondence and requests for materials should be addressed to M.J.S.

nature materials

SUPPLEMENTARY INFORMATION

DOI: 10.1038/NMAT2398

SUPPLEMENTARY INFORMATION:

Biodegradable luminescent porous silicon nanoparticles for *in vivo* applications

Ji-Ho Park, Luo Gu, Geoffrey von Maltzahn, Erkki Ruoslahti, Sangeeta N. Bhatia, & Michael J. Sailor

DOI: 10.1038/NMAT2398

SUPPLEMENTARY METHODS

Preparation of luminescent porous silicon nanopartiels (LPSiNP). Porous silicon samples were prepared by electrochemical etch of a single-crystal, (100)-oriented p-type silicon wafer (0.8-1.2 mΩ cm, Siltronix) by application of a constant current density of 200 mA/cm^2 for 150 s in a 3:1 (v/v) electrolyte of 48 % aqueous HF/ethanol. A freestanding film of the porous silicon nanostructure was then removed from the crystalline silicon substrate by application of a current pulse of 4 mA/cm^2 for 250 s in a solution of 3.3% (by volume) 48 % aqueous HF in ethanol. The freestanding hydrogen-terminated porous silicon film was placed in deionized (DI) water and fractured into multi-sized particles by sonication overnight. The particles were then filtered through a 0.22 μm filtration membrane (Millipore). The nanoparticles were further incubated in DI water for ~ 2 weeks to activate their luminescence in the near-infrared range. Finally, in order to remove dissolved silicic acids during the activation and obtain porous silicon nanoparticles in a size range of 20-200 nm, the activated nanoparticles were spun down in DI water at 14,000 rpm for 30 min, the supernatant containing silicic acids and smaller nanoparticles (< 20 nm) was removed.

For LPSiNP with different porous nanostructures, porous Si samples were prepared by electrochemical etch of a single-crystal, (100)-oriented p-type silicon wafer (0.8-1.2 mΩ cm, Siltronix) by application of a constant current density of 50 mA/cm^2 for 300 s, 200 mA/cm^2 for 150 s or 400 mA/cm^2 for 150 s in a 3:1 (v/v) electrolyte of 48 % aqueous HF/ethanol. A freestanding film of the porous silicon nanostructure was then removed from the crystalline silicon substrate by application of a current pulse of 4 mA/cm^2 for 250 s in a solution of 3.3% (by volume) 48 % aqueous HF in ethanol. The

freestanding hydrogen-terminated porous silicon film was placed in deionized (DI) water and fractured into multi-sized particles by sonication overnight. The particles were then filtered through a 0.22 μm filtration membrane (Millipore). The nanoparticles were further incubated in DI water for ~ 2 weeks to activate their luminescence in the near-infrared range. Finally, in order to remove dissolved silicic acid and obtain porous silicon nanoparticles in a size range of 20-200 nm, the activated nanoparticles in DI water were spun down at 14,000 rpm for 30 min, the supernatant containing silicic acid and non-porous smaller nanoparticles (< 20 nm) was removed.

For LPSiNP with different sizes, the particles were then filtered through a 0.45 μm filtration membrane (Millipore) after overnight sonication process. The nanoparticles were further incubated in DI water for ~ 2 weeks to activate their luminescence in the near-infrared range. First, LPSiNP with larger sizes (hydrodynamic size = ~ 270.3 nm) were obtained by centrifugation at low speed (at 6,000 rpm for 10 min) and removal of the supernatant. The nanoparticles were then filtered through a 0.22 μm filtration membrane. Secondly, LPSiNP with medium size (hydrodynamic size = ~ 125.7 nm, which are the LPSiNP used mainly in this study) were obtained by centrifugation at high speed (at 14,000 rpm for 30 min) and removal of the supernatant. Lastly, LPSiNP with smaller size (hydrodynamic size = ~ 14.5 nm) were obtained from the supernatant.

To prepare D-LPSiNP, a dextran coating was applied. A 1 mL aliquot of an aqueous dispersion of 0.5 mg of LPSiNP was mixed with a 1 mL aliquot of water containing 100 mg of dextran (MW ~20,000, Sigma). The mixture was stirred overnight, rinsed three times using a centrifugal filter (100,000 Da molecular weight cut-off,

DOI: 10.1038/NMAT2398

Millipore, inc.), the particles were resuspended in water and then filtered through a 0.22 μm filtration membrane.

Nanoparticle characterization. Scanning electron micrographs (SEM) were obtained with a Hitachi S-4800 field-emission instrument. A 20 uL drop of ethanol containing LPSiNP was directly placed onto a polished silicon wafer and the solvent allowed to dry in air. Dynamic light scattering (Zetasizer Nano ZS90, Malvern Instruments) was used to determine hydrodynamic size and zeta potential of LPSiNP or D-LPSINP (in DI water). To analyze porous nanostructure (pore surface area, pore size, and pore volume) of LPSiNP, N_2 adsorption isotherms (interpreted with the BJH and BET models) were measured on a Micromeritics Accelerated Surface Area and Prosimetry analyzer (ASAP 2020).

The photoluminescence (PL, λ_{ex} = 370 nm and 460 nm longpass emission filter) and absorbance spectra of LPSiNP or D-LPSiNP in DI water were obtained using a Princeton Instruments/Acton spectrometer fitted with a liquid nitrogen-cooled silicon charge-coupled device detector, and a Hewlett-Packard 8452A UV-vis diode array spectrophotometer, respectively. Fluorescence images of D-LPSiNP in DI water subjected to different excitation wavelength bands were obtained using an IVIS 200 imaging system (Xenogen). (GFP: 445-490 nm and 1 s exposure time, DsRed: 500-550 nm, 2 s exposure time, Cy5.5: 615-665 nm, 8 s exposure time, and ICG: 710-760 nm, 20 s exposure time). The emission filter used was ICG (810-875 nm).

The photostability (photobleaching) of LPSiNP was evaluated relative to organic dyes commonly used in biological imaging (fluorescein, Cy5.5 and Cy7). The LPSiNP

and dyes (dispersed or dissolved in aqueous solution) were illuminated with a 100 W mercury lamp, and fluorescence intensities were monitored using a fluorescence microscope (Nikon Eclipse LV150) equipped with a thermoelectrically cooled CCD camera (Photometrics CoolSNAP HQ^2). Excitation (355 ± 25 nm for LPSiNP, 480 ± 20 nm for Fluorescein, 650 ± 22 nm for Cy5.5, and 710 ± 35 nm for Cy7) and emission (435 nm long pass for LPSiNP, 535 ± 25 nm for Fluorescein, 710 ± 25 nm for Cy5.5, and 800 ± 35 nm for Cy7) were used for these experiments. The fluorescence intensities were monitored at 0.5 or 1 min intervals. The quantum yield (QY) of LPSiNP in ethanol was measured using the comparative method, using Rhodamine 101 (QY = 100%, Sigma) in ethanol as the standard. The Fourier-transform infrared (FTIR) spectra of as-etched porous silicon films and LPSiNP were obtained in the absorption mode using a Thermo Scientific Nicolet 6700 FTIR spectrometer equipped with a diamond Attenuated Total Reflectance (ATR) accessory.

***In vitro* degradation.** A series of samples containing 0.05 mg/mL of LPSiNP or D-LPSiNP in 1 mL of PBS solution were incubated at 37 ºC. An aliquot of 0.5 mL of solution was removed at different time points and filtered with a centrifugal filter (30,000 Da molecular weight cut-off, Millipore, inc.) to remove undissolved LPSiNP. 0.4 mL of the filtered solution was diluted with 4.6 mL HNO_3 (2 %(v/v)) and subjected to analysis by inductively coupled plasma optical emission spectroscopy (ICP-OES, Perkin Elmer Optima 3000DV). The silicon concentration in the original solution was determined by incubating the solution in PBS at 37 ^{o}C for 72 h and measuring the silicon concentration

DOI: 10.1038/NMAT2398

without filtration. The decrease in PL of the above samples over time was also monitored.

Drug loading and cytotoxicity. 0.5 mg LPSiNP (0.5 mg/mL) was mixed with 0.05 mg doxorubicin (DOX, Sigma) in DI water at room temperature overnight and then rinsed three times using a centrifugal filter (100,000 Da molecular weight cut-off, Millipore, inc.). The amount of DOX incorporated into LPSiNP was determined by incubating DOX-loaded LPSiNP (DOX-LPSiNP) in a 0.3 M HCl 70% ethanol solution overnight and comparing the fluorescence with a standard curve (~ 43.8 μg DOX per 1 mg LPSiNP). Release kinetics of DOX from DOX-LPSiNP (0.05 mg/mL) in PBS at 37^{o}C was measured by filtering out DOX-LPSiNP from the solution at each time point using the centrifugal filter and measuring fluorescence of free DOX left in the solution at 590 nm (λ_{ex} = 480 nm).

For drug-mediated cytotoxicity experiments, MDA-MB-435 human carcinoma cells were incubated with LPSiNP, DOX-LPSiNP or free DOX (at different DOX/LPSiNP concentrations) for 48 h and rinsed with cell medium three times. The cytotoxicity of LPSiNP, DOX-LPSiNP or free DOX was evaluated using the MTT assay (Chemicon). For nanostructure- or size-related cytotoxicity experiments (without DOX), HeLa cells were incubated with the LPSiNP (at different LPSiNP concentrations) for 48 h and rinsed with cell medium (no phenol red) three times. The cytotoxicity of LPSiNP was evaluated using the Calcein assay [fluorogenic intracellular esterase sensor Calcein acetoxymethylester (Calcein AM), Invitrogen]. Cell viability was expressed as the percentage of viable cells compared with controls (cells treated with PBS). The

cytotoxicity of the LPSiNP was also examined by observing morphology of live cells using an inverted optical microscope (Nikon).

***In vivo* toxicity, circulation, and bioditribution for free DOX and DOX-LPSiNP.** All animal work was performed in accordance with the institutional animal protocol guidelines in place at the Burnham Institute for Medical Research, and it was reviewed and approved by the Institute's Animal Research Committee. Free DOX or DOX-LPSiNP (in 200 μL PBS solution) were intravenously injected into BALB/c mice at a dose of 2 mg DOX/kg body mass (45.5 mg/kg for LPSiNP of DOX-LPSiNP). To examine preliminary *in vivo* toxicity, body mass of the mice was monitored every 3 days over a period of 3 weeks.

To determine blood half-lives, blood (100 μL) was collected from the periorbital plexus at several different times after injection using heparinized capillary tubes (Fisher), and then immediately mixed with 100 μL of 10 mM EDTA (in PBS) to prevent coagulation. For silicon concentration in the blood (DOX-LPSiNP), the blood samples were digested and prepared as mentioned for the organs. The total silicon concentration in the blood was measured using ICP-OES. For DOX concentration in the blood (free DOX and DOX-LPSiNP), the blood samples were spun down briefly to remove red blood cells and 100 μL of the supernatants was mixed with 100 μL of 0.3 M HCl 70% ethanol solution overnight to extract free DOX molecules from the DOX-LPSiNP. The total DOX concentration in the blood was calculated based on the fluorescence intensity of DOX in the samples (λ_{ex} = 480 nm and λ_{em} = 590 nm).

DOI: 10.1038/NMAT2398

To determine biodistribution of free DOX and DOX-LPSiNP in mouse, the organs (liver, spleen, kidney, lung, heart, and brain) were collected 24 h after injection, weighed, homogenized in 1.5 mL of 0.3 M HCl 70% ethanol solution, and further incubated in the same solution overnight to extract DOX molecules from the organs and DOX-LPSiNP. The homogenized solution was spun down at 10,000 rpm for 10 min and the supernatant was only used to measure the DOX fluorescence. The DOX fluorescence (λ_{ex} = 480nm and λ_{em} = 590 nm) in each tissue was quantified as % injected dose (%ID) per gram of wet tissue.

***In vitro* fluorescence imaging.** HeLa cells (3000 cells per well) were seeded into 8-well chamber glass slides (Lab-Tek) and incubated overnight. A 50 µg per well quantity of LPSiNP was added and the cells incubated for 2 h at 37 ^{o}C in the presence of 10% fetal bovine serum (FBS). The cells were then rinsed three times with cell medium, fixed with 4% paraformaldehyde for 20 min and then observed in the fluorescence microscope (370 nm or 488 nm excitation and 650 nm long pass emission filter) and in the Radiance 2100/AGR-3Q BioRad Multi-photon Laser Point Scanning Confocal Microscope. For confocal fluorescence microscopy, the cells treated with LPSiNP were imaged using 488 nm Ar ion laser excitation and a 650 nm long pass emission filter. For multi-photon fluorescence microscopy, the cells treated with LPSiNP were imaged using 750 nm Mai-Tai laser excitation. The DAPI and LPSiNP signals were separated using 495 dichroic filter and 560 nm long pass filter.

***In vivo* degradation, toxicity, and circulation.** All animal work was performed in accordance with the institutional animal protocol guidelines in place at the Burnham Institute for Medical Research, and it was reviewed and approved by the Institute's Animal Research Committee. LPSiNP or D-LPSiNP (in 200 μL PBS solution) were intravenously injected into BALB/c mice at a dose of 20 mg/kg body mass. For *in vivo* degradation studies, the mice were sacrificed 1 day, 1 week and 4 weeks after injection by cardiac perfusion with PBS under anesthesia, and the brain, heart, kidney, liver, lung, and spleen were collected. The tissues were weighed and then digested with a solution of HNO_3 (0.5 mL, ~15.7 M), H_2O_2 (0.1 mL, 30%) and HF (0.03 mL, 5%) for 2 days. A solution of H_3BO_3 (0.235 mL, 0.4 M) was added and the mixture diluted with HNO_3 (10.50 mL, 2%). The silicon concentration in the samples was determined using ICP-OES.

For the *in vivo* toxicity studies, the mass of each mouse was monitored for 4 weeks after injection and compared with control mice (PBS-injected). The sections of kidney, liver, and spleen tissues harvested from the mice 1 day and 4 weeks after injection were stained with haematoxylin and eosin and then examined by a pathologist. To determine blood half-lives, the blood (100 μL) was collected from the periorbital plexus at several different times after injection using heparinized capillary tubes (Fisher), and then immediately mixed with 100 μL of 10 mM EDTA (in PBS) to prevent coagulation. The blood samples were digested and prepared as mentioned above for the organs. The total silicon concentration in the blood was measured using ICP-OES.

DOI: 10.1038/NMAT2398

***In vivo* fluorescence imaging.** Aliquots of LPSiNP (20 μL of 0.1 mg/mL in PBS) were injected subcutaneously and intramuscularly into the left and right flank, respectively, of a nude mouse, and imaged immediately with GFP excitation (445-490 nm) and ICG emission filter (810-875 nm) using the IVIS 200 imaging system.

For systemic administration, LPSiNP or D-LPSiNP (in 200 μL PBS) were intravenously injected into nude mice at a dose of 20 mg/kg body mass. The mice were imaged under anesthesia several different times after injection using the IVIS 200 imaging system. The organs (bladder, brain, heart, kidney, lymph nodes, liver, lung, skin, and spleen), harvested 24 h after injection, were also imaged. For *in vivo* fluorescence tumor imaging, the nude mouse bearing an MDA-MB-435 human carcinoma tumor (~0.5 cm, one side of flank) was used. The tumor area was imaged under anesthesia several different times after intravenous injection of D-LPSiNP at a dose of 20 mg/kg body mass using the IVIS 200 imaging system. The tumor and muscle around the tumor harvested 24 h after injection, were also imaged. The excitation filters used were GFP (445-490 nm), DsRed (500-550 nm), and Cy5.5 (615-665 nm). The emission filter used was ICG (810-875 nm). For fluorescent histological analysis, sections of liver, spleen, and tumor tissues were fixed with 4% paraformaldehyde, stained with DAPI, and then observed with 370 nm excitation and 650 nm long pass emission filter using the fluorescence microscope.

SUPPLEMENTARY FIGURES

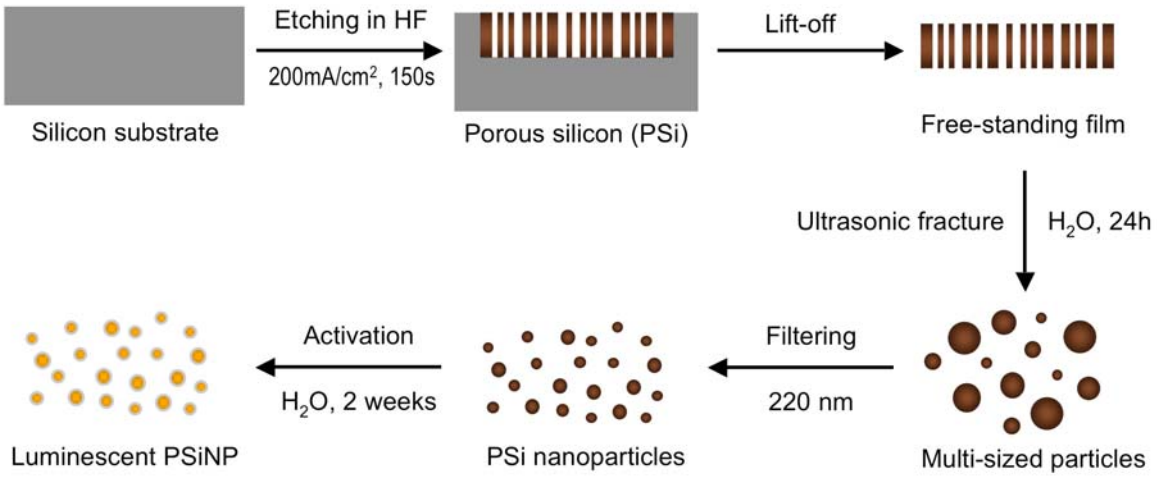

Supplementary Figure 1 Schematic diagram of the synthesis of luminescent porous silicon nanoparticles (LPSiNP). A porous silicon layer with a pore size range of 5-10 nm is first etched into the single-crystal silicon substrate in ethanolic HF solution. The entire porous nanostructure is removed from the Si substrate by application of a current pulse. The freestanding hydrogen-terminated porous silicon film is then placed in an aqueous solution and fractured into multi-sized particles by overnight ultrasonication. The particles are then filtered through a 0.22 μm porous filtration membrane to obtain the porous silicon nanoparticles. Finally, the nanoparticles are incubated in an aqueous solution to activate their luminescence.

DOI: 10.1038/NMAT2398

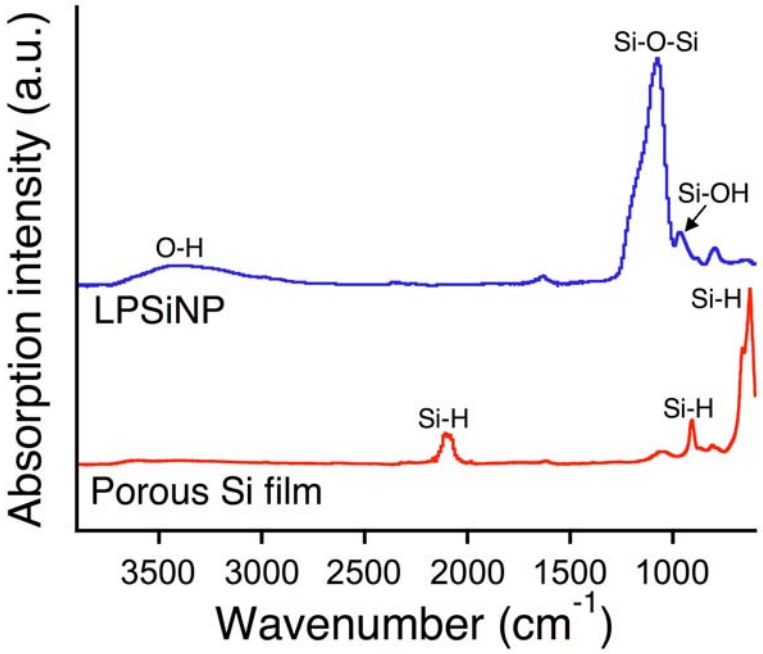

Supplementary figure 2 FTIR spectra of porous silicon film and luminescent porous silicon nanoparticles (LPSiNP) shown in **Supplementary Fig. 1.** The hydrogen-terminated surface of the as-etched porous silicon film is converted to silicon dioxide in the porous silicon nanoparticles. The oxide layer passivates the nanoparticle surface and also generates interfacial oxides, giving rise to a strong NIR photoluminescence.

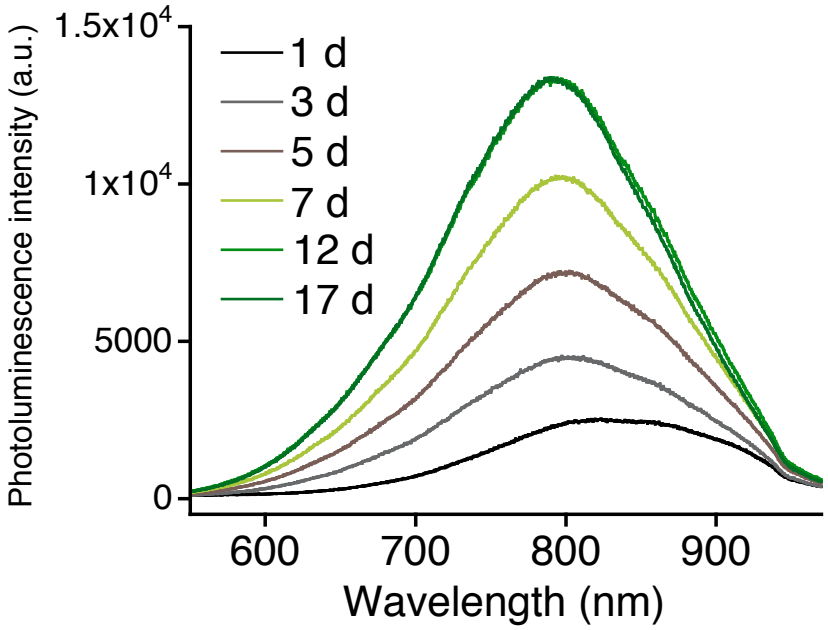

Supplementary figure 3 Photoluminescence spectra of LPSiNP, acquired during activation in deionized (DI) water at room temperature (1 d indicates 1 day after immersion in DI water). Note the increase in PL intensity and slight blue-shifting of the peak maximum with time.

DOI: 10.1038/NMAT2398

a

sample	size (nm)*	etching conditions	SEM image	SEM pore size** (nm)	BET pore surface area† (m^2/g)	BET pore width§ (nm)	BET pore volume§ (cm^3/g)
LPSiNP-50	132.5±12.3	50 mA/cm^2 for 300 sec		7.4 ± 2.3	471	7.32	1.07
LPSiNP-200	125.7±9.7	200 mA/cm^2 for 150 sec		9.3 ± 2.7	648	7.67	1.32
LPSiNP-400	122.6±14.5	400 mA/cm^2 for 150 sec		18.1 ± 5.2	495	7.79	1.15

100 nm

*The size was analyzed using dynamic light scattering (DLS).

** The pore size was analyzed with the image taken from top view (n > 10). The data did not include sizes of smaller pores interconnected between main pores.

† The surface area was analyzed with BET method.

§ The pore width and pore volume were analyzed with BJH method.

b

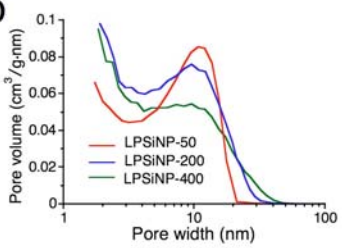

c

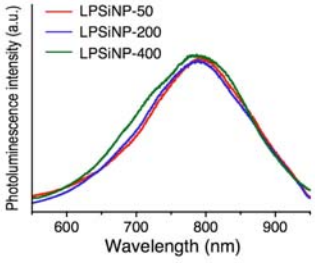

d

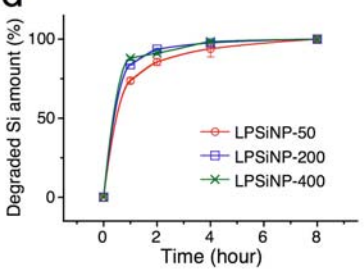

e

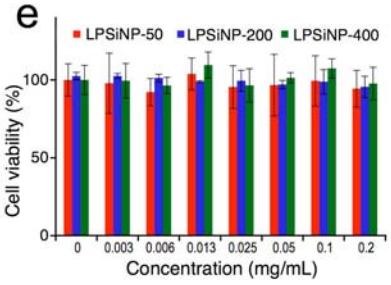

Supplementary figure 4 Characterization of three types of LPSiNP prepared with different porous nanostructures. (a) Analysis of porous nanostructures of LPSiNP by SEM and gas adsorption (BET/BJH) methods. The particle size values (by Dynamic Light Scattering, DLS) are the means plus/minus one standard deviation for three batches of LPSiNP, and the pore size values (by SEM) are averages of > 10 different pores from randomly selected LPSiNP. (b) Pore size distributions and pore volume in LPSiNP determined by gas adsorption (BJH and dV/dw methods). (c) Photoluminescence spectra of LPSiNP (λ_{ex} = 370 nm). (d) *In vitro* degradation of LPSiNP in PBS solution at 37°C as a function of time. Note that LPSiNP prepared using the etching condition with a current density of 50 mA/cm^2 show slightly slower degradation relative to the other two preparations of LPSiNP, suggesting that the their lower porosity may be responsible for the slower degradation. (e) Cytotoxicity of LPSiNP by calcein assay. HeLa cells were incubated with LPSiNP for 48 h and then viability was evaluated using the fluorogenic intracellular esterase sensor calcein acetoxymethylester (Calcein AM).

a

Sample	size (nm)	zeta potential (mV)	blood half-life (min)
LPSiNP-S	14.5 ± 5.1	- 52.3 ± 4.8	11.9 ± 1.7
LPSiNP-M	125.7 ± 9.7	- 52.0 ± 2.8	27.6 ± 1.8
LPSiNP-L	270.3 ± 10.3	- 50.5 ± 7.1	< 5

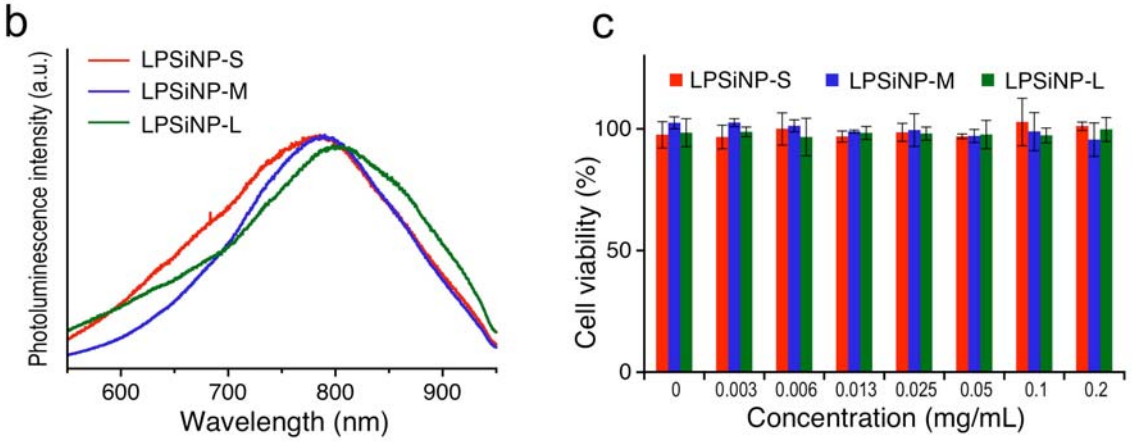

Supplementary figure 5 Characterization of LPSiNP with different average particle sizes, prepared using the same etching conditions (200 mA/cm^2 for 150 sec). The suffixes "-S" "-M" and "-L" refer to small (15 nm), medium (126 nm), and large (270 nm) particles. (a) Effect of nanoparticle size on the blood circulation half-life in mouse (n = 3). Note that the LPSiNP-M show the longest circulation times relative to LPSiNP with other sizes. The LPSiNP-S are cleared rapidly by the kidney due to their small size (close to the typical renal clearance range of < 5.5 nm) while the LPSiNP-L are cleared rapidly by the spleen or lung non-specifically due to their large size. The size and zeta potential values obtained by DLS are the means plus/minus one standard deviation for three lots of LPSiNP. The blood half-life values were obtained by fitting the concentration of silicon in each blood sample at each time point to a single-exponential equation using a one-compartment open pharmacokinetic model[1]. (b) Photoluminescence spectra of the LPSiNP with different sizes (λ_{ex} = 370 nm). (c) Cytotoxicity of the LPSiNP with different sizes by Calcein assay. HeLa cells were incubated with LPSiNP for 48 h and then their viability was evaluated using the fluorogenic intracellular esterase sensor Calcein acetoxymethylester (Calcein AM).

DOI: 10.1038/NMAT2398

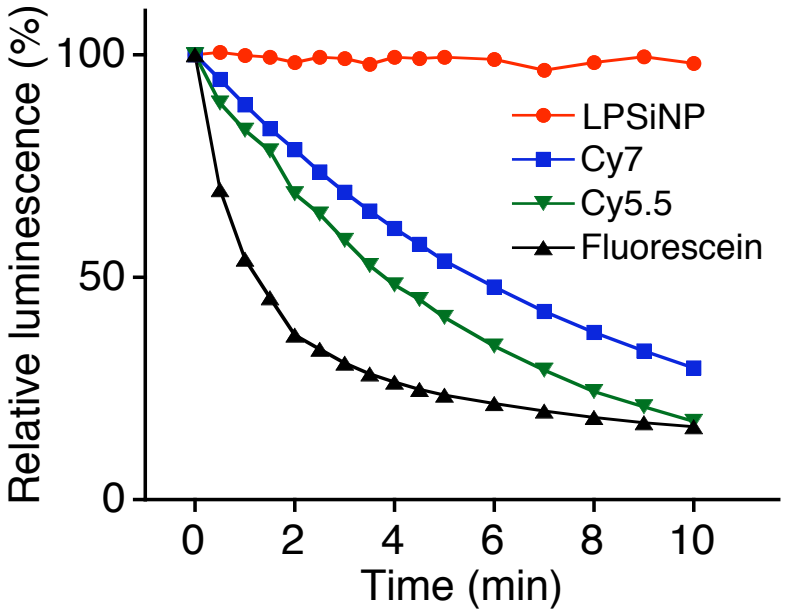

Supplementary figure 6 Changes in fluorescence intensity of LPSiNP dispersed in aqueous solution exposed to air during continuous exposure to a 100 W mercury lamp, compared with organic dyes commonly used in biological imaging experiments (Cy5.5, Cy7, and fluorescein). Excitation wavelengths of 355 ± 25 nm for LPSiNP, 480 ± 20 nm for fluorescein, 650 ± 22 nm for Cy5.5, and 710 ± 35 nm for Cy7, and emission wavelengths of 435 nm (long pass) for LPSiNP, 535 ± 25 nm for fluorescein, 710 ± 25 nm for Cy5.5, and 800 ± 35 nm for Cy7 were used for these experiments. The fluorescence intensities were monitored with a thermoelectrically cooled CCD camera.

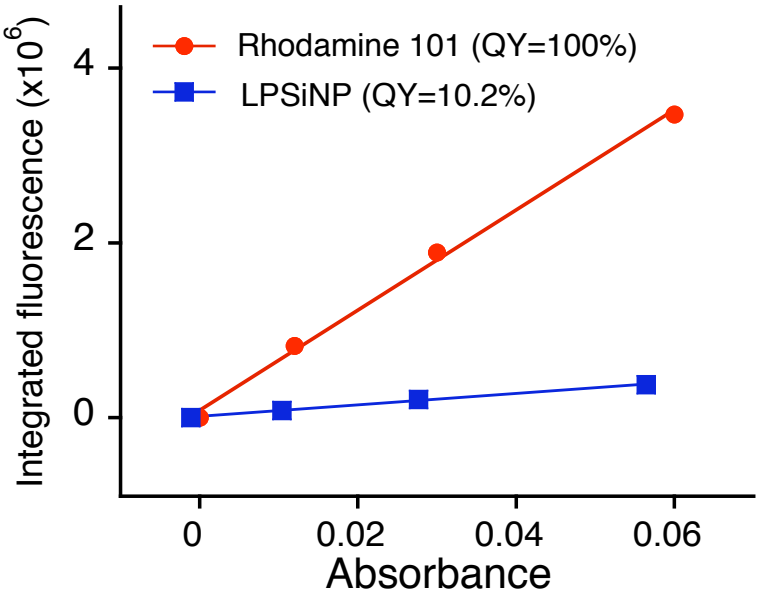

Supplementary figure 7 Quantum yield (QY=10.2%) of luminescent porous Si nanoparticles (LPSiNP) compared to Rhodamine 101 (QY=100%)[2].

DOI: 10.1038/NMAT2398

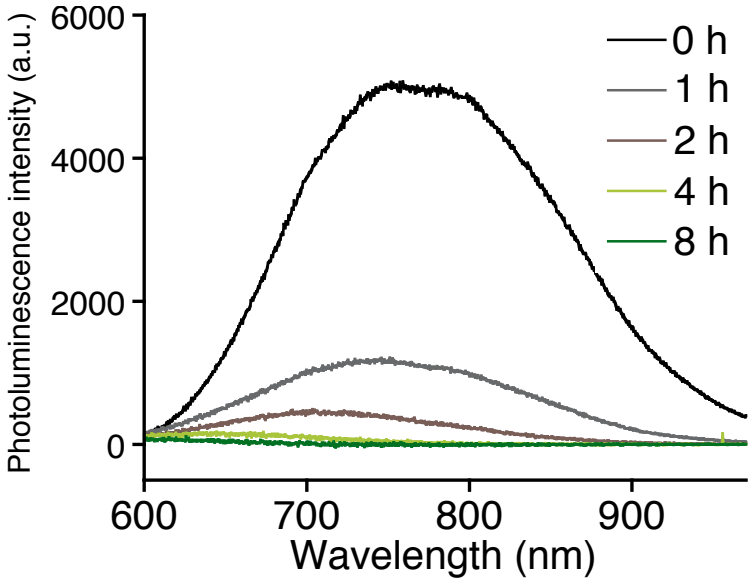

Supplementary figure 8 Evolution of photoluminescence spectrum of LPSiNP during degradation under physiological conditions (in PBS at 37 ^{o}C). The maximum intensity of the photoluminescence spectrum at each time point was used for **Fig. 1d**.

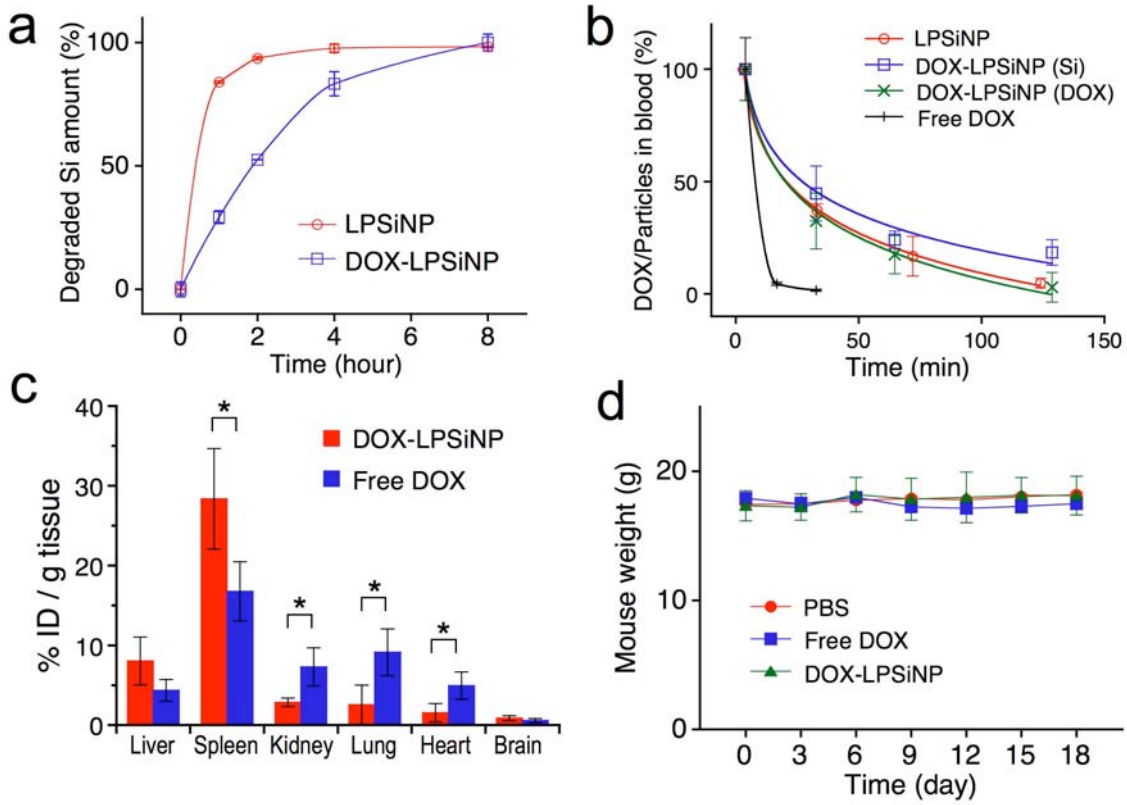

Supplementary figure 9 Characterization of DOX-loaded LPSiNP (DOX-LPSiNP). Zeta potential of LPSiNP increases from - 52 mV to - 39.1 mV after DOX loading. (a) Appearance of silicon in solution (by ICP-OES) from a sample of LPSiNP and DOX-LPSiNP incubated in PBS solution at 37°C as a function of time. (b) Blood concentration of silicon (by ICP-OES) or DOX (by fluorescence) for mice injected with LPSiNP, DOX-LPSiNP, or free DOX as a function of time (n = 3). DOX in DOX-LPSiNP were able to circulate for a longer period of time than free DOX by incorporating DOX in the porous nanostructure of LPSiNP. Note that there is no significant difference in the circulation times between DOX-LPSiNP and LPSiNP. (c) Biodistribution of DOX from mice (n = 3) injected with free DOX or DOX-LPSiNP. The tissues were homogenized 24 h after single intravenous injection of free DOX or DOX-LPSiNP (concentration of DOX in all experiments was 2 mgDOX/kg, corresponding to 45.5 mg/kg of LPSiNP in the DOX-LPSiNP formulation) and the DOX fluorescence (λ_{ex} = 480nm and λ_{em} = 590 nm) in each tissue was analyzed as % injection dose (%ID) per gram of wet tissue. The results show that biodistribution of DOX from DOX-LPSiNP is similar to that of LPSiNP as shown in figure 2b, confirming that LPSiNP retain the loaded DOX during the circulation. In contrast, a significant amount of free DOX accumulated in kidney, lung, and heart, which may induce *in vivo* acute or chronic toxicity (*$p < 0.05$). (d) Body mass change in mice injected with free DOX, and DOX-LPSiNP (concentration of DOX in all experiments was 2 mgDOX/kg, corresponding to 45.5 mg/kg of LPSiNP in the DOX-LPSiNP formulation) compared with PBS control (n = 3). There was no statistically significant difference in the weight change between control (PBS), free DOX, and, DOX-LPSiNP over a period of 3 weeks.

DOI: 10.1038/NMAT2398

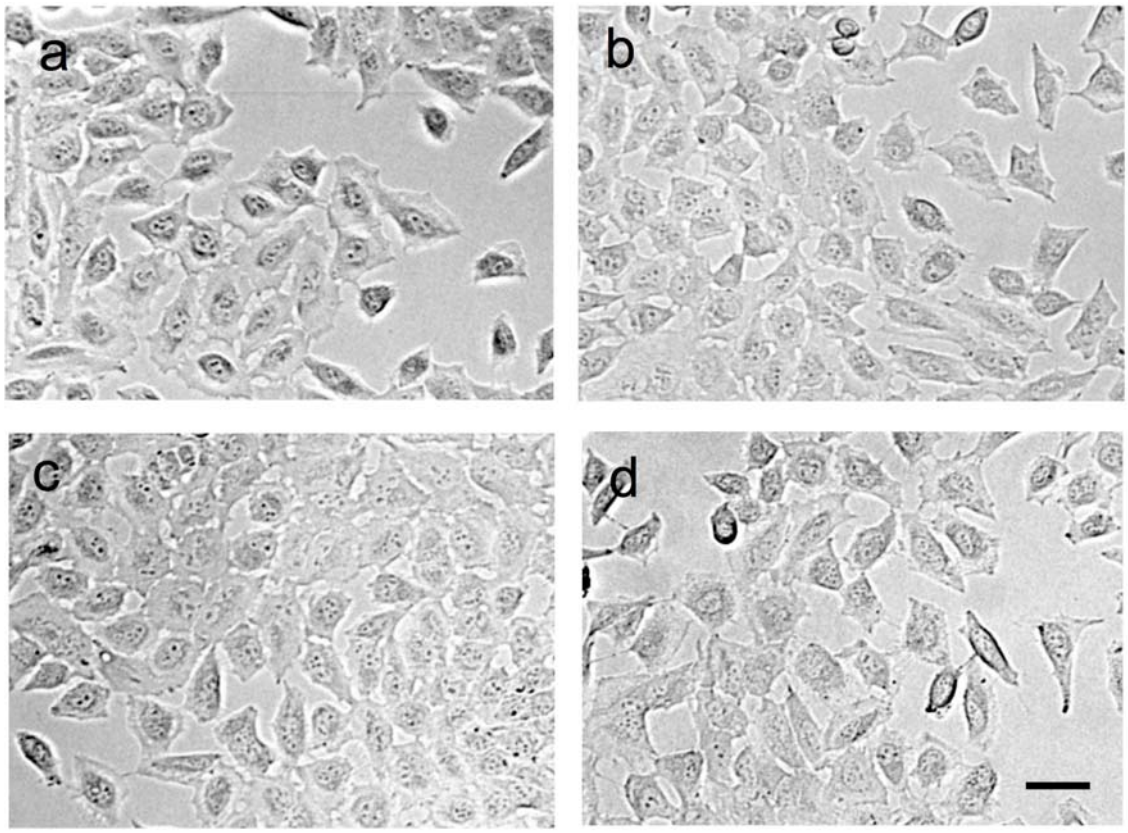

Supplementary figure 10 Optical microscope images of HeLa cells incubated with LPSiNP at a concentration of (a) 0 mg/mL, (b) 0.013 mg/mL, (c) 0.05 mg/mL, and (d) 0.2 mg/mL. The cells were rinsed three times using cell medium (no phenol red) 48 h after incubation and immediately imaged using an inverted optical microscope. The scale bar is 20 μm.

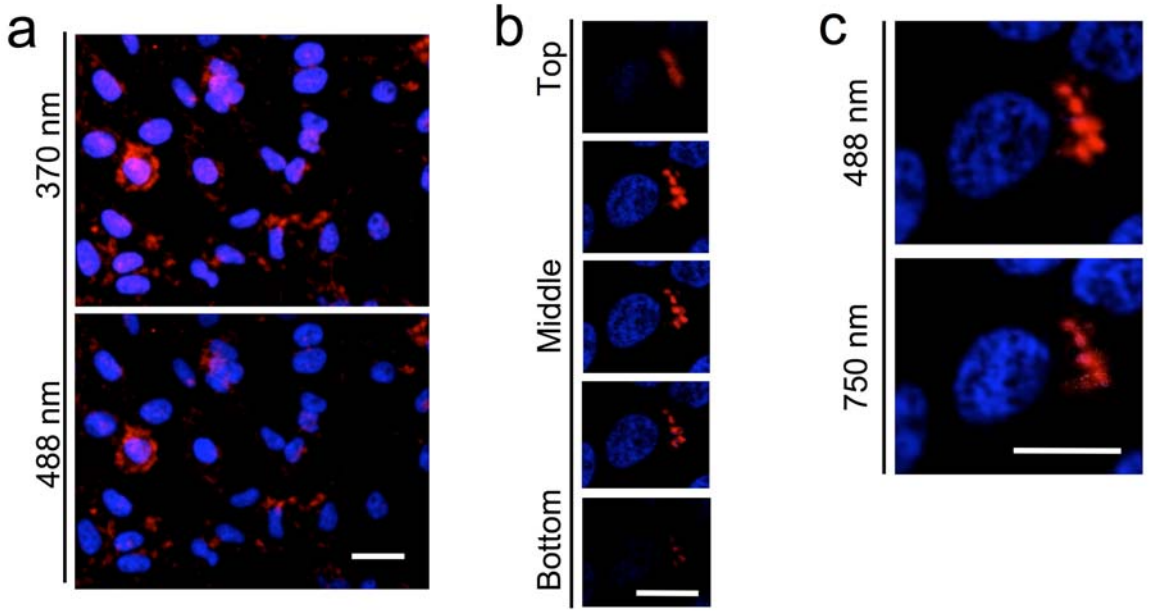

Supplementary figure 11 *In vitro* cellular imaging with LPSiNP. HeLa cells were treated with LPSiNP for 2 h, fixed and then imaged. (a) Fluorescence microscope images of cellular uptake and binding of LPSiNP. The nanoparticles can be imaged *in vitro* under both excitation wavelengths indicated on the left side of the images (λ_{em} = 650 nm long pass). (b) Confocal fluorescence microscope images of cellular uptake of LPSiNP (λ_{ex} = 488 nm and λ_{em} = 650 nm long pass). (c) Multi-photon fluorescence microscope image of celluar uptake of LPSiNP (λ_{ex} = 750 nm). The LPSiNP are clearly observable inside the cells under two-photon excitation conditions as well as with single-photon excitation, in agreement with previous observations with porous silicon chips[3]. The scale bar is 20 μm.

DOI: 10.1038/NMAT2398

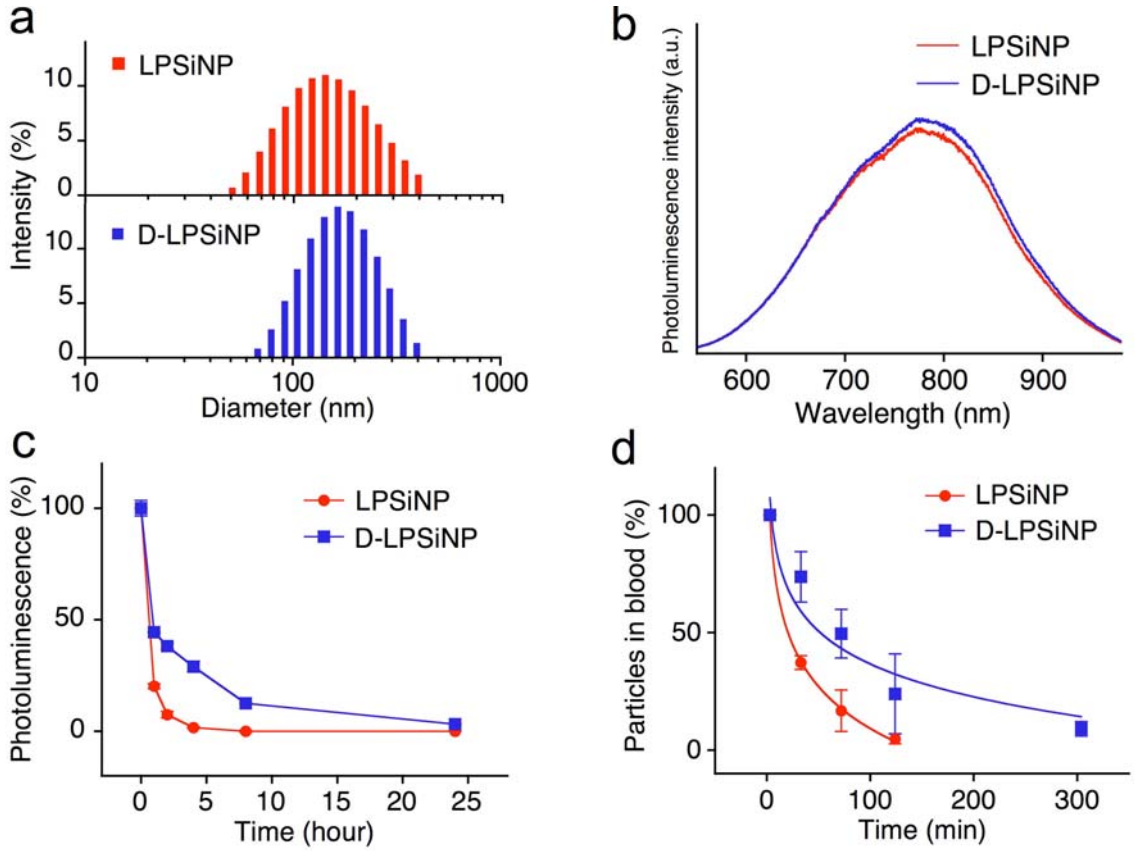

Supplementary figure 12 Characterization of dextran-coated luminescent porous silicon nanoparticles (D-LPSiNP). (**a**) Dynamic light scattering size data obtained from LPSiNP and D-LPSiNP. Note that the size and zeta potential increases from 125 nm to 151 nm and from -52 mV to -43.5 mV after dextran coating, respectively. Although these samples display a relatively large size distribution, there are several FDA (US Food and Drug Administration)-approved nanoparticle formulations that span this range, such as liposomal doxorubicin (Doxil®), albumin-bound Paclitaxel (Abraxane®), and dextran-coated iron oxide nanoparticles (Feridex®). (**b**) Photoluminescence spectra of LPSiNP and D-LPSiNP with UV excitation (λ = 370 nm). (**c**) *In vitro* degradation of LPSiNP and D-LPSiNP (in PBS at 37 ^{o}C). Degradation is monitored as the intensity of photoluminescence from the nanoparticle. (**d**) Blood concentration of silicon (by ICP-OES) for mice (n = 3) injected with LPSiNP or D-LPSiNP as a function of time. LPSiNP are cleared in a short time (blood half-life: 27.6 ± 1.8 min) while D-LPSiNP circulate for a longer period of time (blood half-life: 82.0 ± 15.8 min).

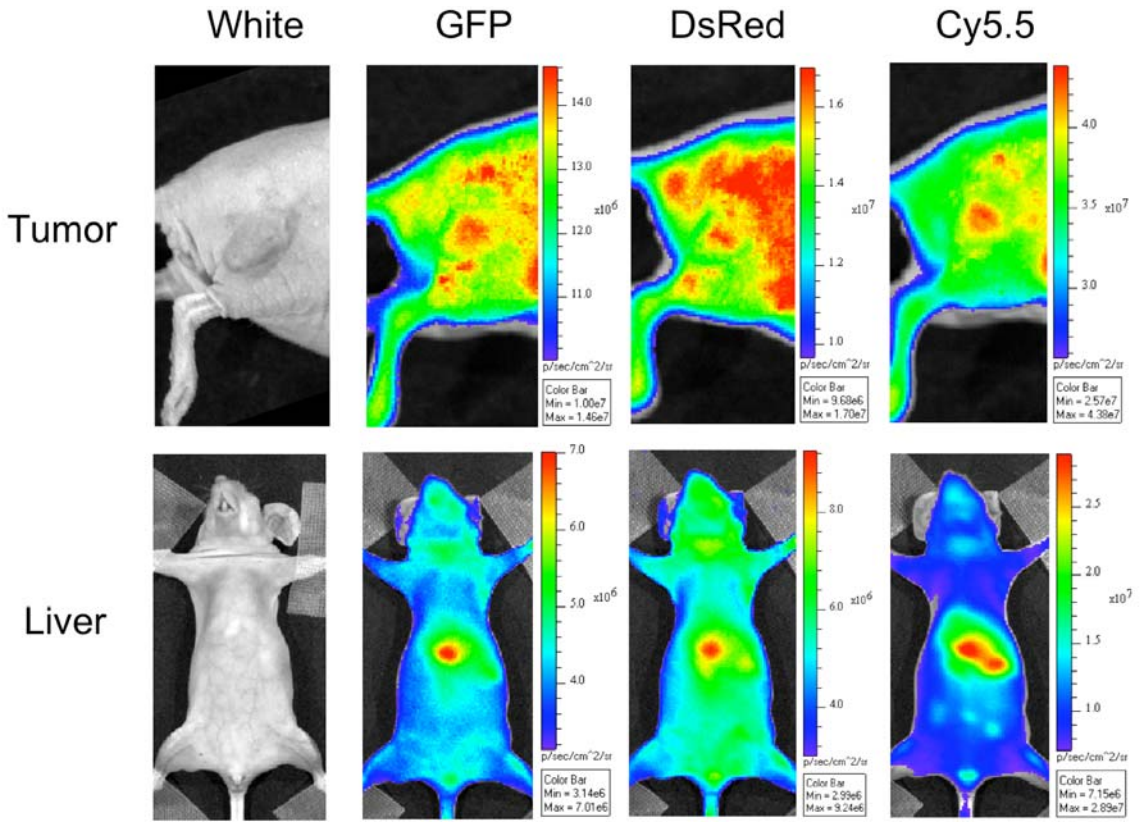

Supplementary figure 13 Fluorescence images of mouse bearing MDA-MB-435 tumor after injection of dextran-coated luminescent porous silicon nanoparticles (D-LPSiNP) using different excitation filters (GFP: 445-490 nm, DsRed: 500-550 nm, Cy5.5: 615-665 nm, and 20 s exposure time for all images). The mouse was imaged 8 h after intravenous injection of D-LPSiNP (20 mg/kg). The emission filter used is ICG (810-875 nm).

DOI: 10.1038/NMAT2398

References Cited

1. Wunderbaldinger, P., Josephson, L. & Weissleder, R. Tat peptide directs enhanced clearance and hepatic permeability of magnetic nanoparticles. *Bioconjugate Chem.* **13**, 264-268 (2002).
2. Williams, A.T.R., Winfield, S.A. & Miller, J.N. Relative fluorescence quantum yields using a computer controlled luminescence spectrometer. *Analyst* **108**, 1067-1071 (1983).
3. Chin, R.P., Shen, Y.R. & Petrova-Koch, V. Photoluminescence from porous silicon by infrared multiphoton excitation. *Science* **270**, 776-778 (1995).